

Scalable Physics-Informed Neural Networks for Accelerating Electromagnetic Transient Stability Assessment

Ignasi Ventura Nadal*, Mohammad Kazem Bakhshizadeh[†], Petros Aristidou[‡],
Nicolae Darii*, Rahul Nellikkath*, and Spyros Chatzivasileiadis*

* Department of Wind and Energy Systems, Technical University of Denmark, Kgs. Lyngby, Denmark

[†] Ørsted Wind Power A/s, Fredericia, Denmark

[‡] Sustainable Power Systems Lab, Cyprus University of Technology, Limassol, Cyprus

Emails: {ignad, nidar, rnelli, spchatz}@dtu.dk, modow@orsted.com, petros.aristidou@cut.ac.cy

Abstract—This paper puts forward a framework to accelerate Electromagnetic Transient (EMT) simulations by replacing individual components with trained Physics-Informed Neural Networks (PINNs). EMT simulations are considered the cornerstone of transient stability assessment of power systems with high shares of Inverter-Based Resources (IBRs), and, although accurate, they are notorious for their slow simulation speed. Taking a deeper dive into the EMT simulation algorithms, this paper identifies the most computationally expensive components of the simulation and replaces them with fast and accurate PINNs. The proposed novel PINN formulation enables a modular and scalable integration into the simulation algorithm. Using a type-4 wind turbine EMT model, we demonstrate a 4–6x simulation speedup by capturing the Phase-Locked Loop (PLL) with a PINN. We validate all our results with PSCAD software.

Index Terms—differential-algebraic equations, electromagnetic transient simulation, physics-informed neural networks, wind power integration

I. INTRODUCTION

The rapid expansion of Inverter-Based Resources (IBRs) in modern power systems, such as wind farms, photovoltaic systems, or batteries, has led to a significant increase in the computational requirements and costs associated with stability studies. For decades, power systems have relied on synchronous generators. IBRs pose a complete paradigm shift, based on a different technology that purely relies on control logic and high-frequency switching semiconductors. This shift presents a fundamental challenge to the power system industry, as fast-reacting and complex IBR dynamics replace the slow electromechanical ones [1–3]. Thus, time-domain simulations, the core method for stability studies, are caught between two opposing forces. On the one side, grid operators require more simulations and scenarios to ensure system reliability. On the

other side, the cost of the required simulations drastically increases, as they feature more detailed and sophisticated models that often need Electromagnetic Transient (EMT) modeling.

While a few ideas have been proposed to address the rising cost of the much-needed time-domain simulations [4], the core of the simulation algorithms still remains untouched. The most applied approach, so far, has been using more powerful and dedicated hardware, which also opened the door to real-time simulations [5, 6] and the parallelization of some processes [7, 8]. However, the primary methods used to simulate are the same.

New methods are needed to improve simulation performance. Physics-Informed Neural Networks (PINNs) have recently emerged as a powerful, fast, and flexible computational paradigm for capturing complex physical systems with high fidelity [9, 10]. By embedding physical laws into the learning process, PINNs can accurately represent nonlinear system behaviors over extended time periods. These features make PINNs highly attractive for power system simulations as a new computing method that can significantly accelerate time-domain simulations.

Several works have addressed how to leverage PINNs to accelerate power system Root Mean Square (RMS) simulations, often known as phasor-type simulations [11–14]. However, their applicability to EMT studies has remained an open question. The challenges associated with the highly nonlinear, sophisticated, and oscillatory nature of EMT simulations make PINN modeling very complex. This paper introduces a new methodology that enables a modular and efficient integration of PINNs for faster EMT simulations. PINNs, trained on the underlying physical equations, capture the closed-form solution of the most computationally intensive control logic, significantly reducing the computational burden at every time step. The contributions of this paper are as follows:

- We propose a modular integration of Physics-Informed Neural Networks (PINNs) into existing power system time-domain simulators, identifying computational bottlenecks and replacing them with trained PINN surrogates for both RMS and EMT simulations.

Submitted to the 24th Power Systems Computation Conference (PSCC 2026). This work was supported by the ERC Starting Grant VeriPhIED, Grant Agreement 949899, and the ERC Proof of Concept PINNSim, Grant Agreement 101248667, both funded by the European Research Council. This work was supported by the Horizon Europe MSCA programme, Grant Agreement 101073554, funded by the Horizon Europe MSCA programme.

- We introduce an explicit PINN formulation, consistent with state-of-the-art EMT software, that captures nonlinear closed-loop control blocks and provides a direct solution without time delays or iterative solvers, thereby reducing the execution burden.
- We integrate the formulation into an EMT solver for a standardized type-4 wind turbine, replacing the PLL, and demonstrate 4–6x acceleration with high accuracy across scenarios, with validation against PSCAD.

The code is made available online to foster the adoption of PINNs in the power systems community [15].

The remainder of this paper is structured as follows. Sec. II defines the vision for a modular and efficient integration of PINNs for power systems simulations. In the following sections, the focus shifts to the EMT simulation application. Sec. III describes the EMT simulation framework and proposes PINNs as an accurate and fast alternative. Sec. IV explains how PINNs are formulated and trained. Numerical results using a wind turbine type-4 EMT model are presented in Sec. V. Conclusions are provided in Sec. VI.

II. ACCELERATING TIME-DOMAIN SIMULATIONS

In this section, we describe how we envision the integration of PINNs into the power systems simulation framework to accelerate simulations in a reliable and practical manner.

A. The vision

PINNs have several characteristics that make them highly attractive to power system simulations. They can accurately learn nonlinear dynamics over large time steps and provide a fast, explicit, direct-solution model, thereby avoiding traditional stepping algorithms. Leveraging these characteristics is still an open research question for the power systems industry. One approach is to develop a new data-driven solver entirely based on PINNs. This was first explored in [11], showing significant speed-ups but requiring widespread PINN adoption. A second approach is to modularly integrate these speed-ups into the existing simulation framework [12]. This approach can still achieve significant speed-ups while remaining compatible with existing tools, and is therefore widely applicable.

Following the modular integration of PINNs into existing state-of-the-art simulators, our vision is to create an automated process: we analyze the desired simulated power system, assess where the main bottlenecks are, and replace them with a PINN. This integration would enable the user to decide before running the simulation whether to use a PINN acceleration technique and what the expected speed-up is. Fig. 1 illustrates this concept. The power system simulation tool contains the core algorithm that gathers all component models, simulates the entire system over time, and handles the pre-processing and post-processing. The component models define the power system. The width of the arrows from each component represents the complexity they introduce to the simulation tool. The integration framework targets the component models that pose the biggest challenge to the simulation tool, and trains PINNs that can accurately replace those components and simplify the

computational burden. This vision applies to all types of power system dynamic simulations.

B. RMS vs. EMT

We classify power system simulations into two groups: *RMS simulations* and *EMT simulations*. This classification, similar to [16], groups simulations by modeling detail. RMS simulations assume steady-state operation of the network, using phasors to capture electromechanical deviations. By contrast, EMT simulations model the waveforms of all phases across the system, requiring more detailed and sophisticated models. Therefore, EMT simulations are significantly more computationally expensive but capture dynamics over a broad band of frequencies. Despite fundamental differences between these two groups, the simulation speed of both algorithms mostly comes down to two factors: (i) how many time steps are required, and (ii) how much time it takes to evaluate all the system models in each time step.

In RMS simulations, the system models are relatively simple, as they typically use a positive-sequence single-phase equivalent. Thus, the dominant time cost comes from the number of time steps required, which is determined by how large the time steps are. Traditional methods quickly become inaccurate when the step size increases, limiting the solver's step sizes and ultimately the simulation speed. PINNs, on the other hand, once trained with the underlying component dynamics, provide accurate representations for large steps. Considering that the fast-evolving components are the ones that constrain the maximum accurate step size, we can train PINNs for these fast components and achieve larger simulation step sizes without losing accuracy, as shown in [14].

In EMT simulations, the time steps must be extremely small to accurately capture the dynamics of the RLC circuits. These dynamics show very fast and intricate interactions and cannot be easily captured with purely data-driven methods. However, in EMT, the evaluation time of the system models becomes a major contributor to runtime, as the nonlinear control models often require iterative solvers. PINNs can provide significant speed-ups by replacing these complex control

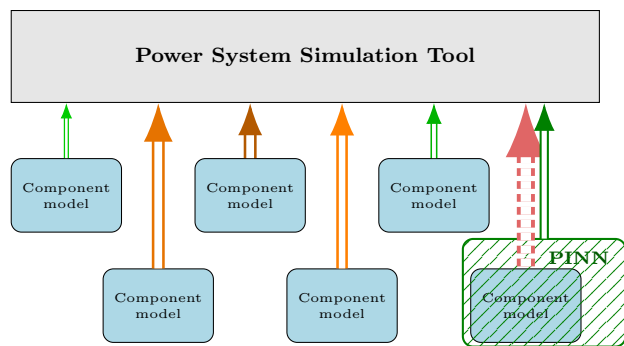


Fig. 1: Represented is the PINN integration vision for faster simulations. We first identify which components have the biggest computing burden in the simulation, and replace them with a PINN.

blocks, providing a fast and explicit solution to closed-loop nonlinear equations. In this work, we introduce, for the first time, a PINN formulation that modularly integrates into EMT solvers, replacing computationally intensive models with fast and accurate PINNs.

III. EMT SIMULATIONS

In this section, we formulate the generic power system time-domain simulation problem and describe the EMT simulation formulation and algorithm.

A. Generic formulation

Time-domain simulations are defined by two parts: (i) the component models, which describe the physics and control of each component in the system; and (ii) an integration algorithm, which numerically integrates all models step by step until the simulation ends. All the component models create a system of linear and nonlinear Differential-Algebraic Equations (DAEs) that together replicate the behaviour of the power generation components, networks, sources, control systems, and protection devices. The system has the following form:

$$\mathbf{F}(\dot{\mathbf{x}}(t), \dot{\mathbf{y}}(t), \mathbf{x}(t), \mathbf{y}(t), \mathbf{u}(t), \mathbf{m}, \mathbf{n}, t) = 0, \quad (1)$$

where $\mathbf{x}(t)$ represents the differential states of the network equations, and $\mathbf{y}(t)$ represents the differential states of the device model equations. $\mathbf{u}(t)$ represents the algebraic states of the device models. Array \mathbf{m} captures the parameters present in the network equations, and \mathbf{n} in the device equations [17].

To solve this set of equations over time, a numerical integrator approximates the evolution of the system's differential equations from a current value $\mathcal{X}_{t-\Delta t} = \{\mathbf{x}_{t-\Delta t}, \mathbf{y}_{t-\Delta t}, \mathbf{u}_{t-\Delta t}\}$ to the future value $\mathcal{X}_t = \{\mathbf{x}_t, \mathbf{y}_t, \mathbf{u}_t\}$ constrained by the system's algebraic equations.

B. EMT simulation problem

EMT simulations replicate power system dynamics with very high detail. The modeling captures the full waves of each phase throughout the entire simulation, representing the dynamic behaviour of the lines. Assuming the basic circuit formulation with lumped elements, the network's state variables $\mathbf{x}(t)$ from (1) become the network voltages $v(t)$ and currents $i(t)$. The relationship between the two is described in (2) through resistance R , inductance L , and capacitance C elements.

$$v_k(t) - v_m(t) = Ri_{km}(t) \quad (2a)$$

$$v_k(t) - v_m(t) = L \frac{d}{dt} i_{km}(t) \quad (2b)$$

$$C \frac{d}{dt} (v_k(t) - v_m(t)) = i_{km}(t). \quad (2c)$$

The control systems, represented by $\mathbf{y}(t)$ and generally defined with block diagrams, represent the interconnections between system elements.

C. EMT simulation program

There are several approaches to solve an EMT simulation problem. In this work, we consider the partitioned algorithm, used in most state-of-the-art power system software. This algorithm divides the EMT simulation problem into two parts, the electric network and the control systems [18].

1) *Electrical systems*: The electrical system solution is based on the principles outlined by H.W. Dommel in [19, 20]. The differential equations of the circuit elements in (2) are transformed into linearized algebraic equations by discretizing them with the trapezoidal rule. The resulting equations define the so-called companion models and depend on voltage, current, and past values. Fig. 2 depicts the companion models of an inductance and a capacitance. See [18] for more details on the transformation.

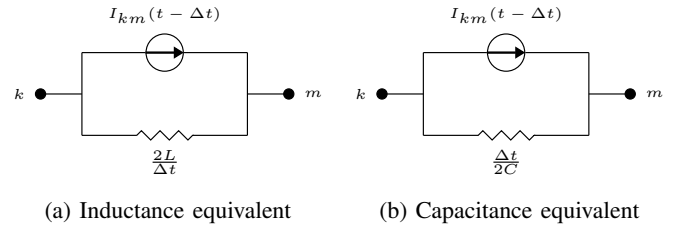


Fig. 2: Companion circuits of an inductance and a capacitance.

The companion models of all network elements and the electrical circuits of all connected components are used to build the nodal admittance equations. Assembled together, they yield the network solution in the form

$$\mathbf{Y}\mathbf{v}(t) = \mathbf{i}(t) - \mathbf{I}(t), \quad (3)$$

where $\mathbf{v}(t)$ are the bus voltages, $\mathbf{i}(t)$ the branch currents, and $\mathbf{I}(t)$ the history currents. \mathbf{Y} is the symmetric nodal admittance matrix. Nonlinear electrical elements, such as transformers or surge arresters, can also be included in this formulation [18].

2) *Control systems*: The control systems of all devices in the system, usually defined by block diagrams, are solved together. These primarily include converters, excitation systems, and protective relays. The control systems solution algorithm, first proposed in [21] and labeled as TACS, also uses the trapezoidal rule to discretize its differential equations. How the control systems are solved then depends on the type of resulting system. The three possible types are solved as follows: (i) linear systems are solved analytically, (ii) systems with nonlinearities only in open-loop paths are solved sequentially, and (iii) systems where nonlinearities appear in closed loops require an iterative method or the introduction of a time delay to break the feedback loop.

Most EMT models result in the latter type, where nonlinearities appear in closed loops. The fastest and most common approach to solving such systems is to introduce a time delay in the feedback, thereby opening the loop to allow for a non-iterative sequential solution. The main shortcoming of this approach is reduced accuracy, and it can lead to instability in otherwise physically stable simulations [22, 23]. The most

accurate approach is to use an iterative method to solve the closed-loop system; however, this approach has a higher computational cost. Fig. 3 illustrates both approaches.

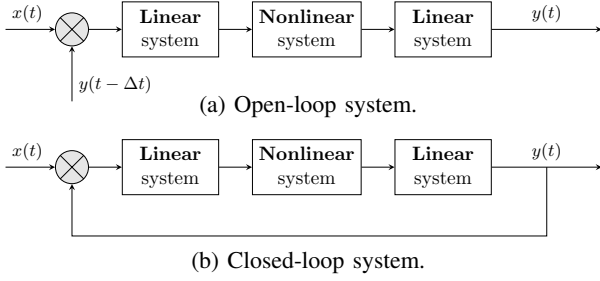


Fig. 3: The two main approaches to solve control systems.

3) *Interface network-control solutions*: The high efficiency of the electric system solution, which leverages the symmetrical properties of the nodal matrix \mathbf{Y} , motivates solving the electric and control systems separately. The control systems are nonlinear and asymmetric, requiring more computational effort. The exchange of information between the two is done sequentially; thus, the network solution always uses the control system's outputs delayed by one time step. Fig. 4 depicts this structure. The network is solved from $t - \Delta t$ to t using the control inputs from the past step, $t - 2\Delta t$ to $t - \Delta t$. Then, the control systems are calculated with the updated electric solution from $t - \Delta t$ to t .

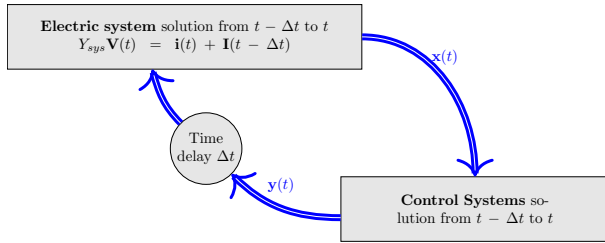


Fig. 4: Interface overview between the network and control systems solution [20].

D. Accelerating the control systems solution with PINNs

As explained in Sec. III-C, the EMT simulation algorithm solves the electrical network and control systems separately in each time step. The electrical network solution becomes a highly efficient computation. In contrast, the control systems solution is slow due to the unstructured nature of the equations and the nonlinearities in closed loops that are difficult to handle. PINNs can accurately capture the dynamics of these nonlinear closed loops, thus offering an alternative to open- and closed-loop solutions. By training with the underlying equations, PINNs provide a fast and explicit solution to the nonlinear closed loop without requiring a time delay. Fig. 5 illustrates the proposed integration. The PINN requires the same inputs and yields the same outputs as the captured control system. This modular approach allows training for part of, or several parts of, any control system. Once the PINN has

been accurately trained for a broad input range, it can be integrated into any simulation, scenario, and system with the same architecture. Sec. IV details how PINNs are trained and integrated into the simulation framework.

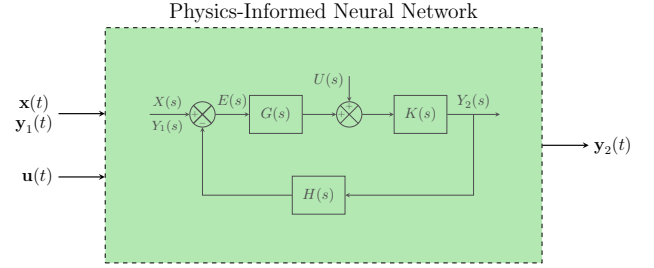


Fig. 5: PINNs can accurately capture the dynamics of nonlinear closed-loop control systems.

IV. NEURAL NETWORKS INTEGRATION

This section defines PINNs and establishes them as an explicit nonlinear solver, describing their input domain and training procedure.

A. General formulation

To parametrize a PINN, we use a fully connected feedforward Neural Network (NN) with K hidden layers and N_k neurons in each layer [24]. Each hidden layer k comprises the weight matrices W^k and bias vectors b^k . Together, they define the set of learnable parameters of the PINN, $\Theta = [W^k, b^k]$. The relation between inputs and outputs is defined by

$$z_{k+1} = \sigma(W^{k+1}z_k + b^{k+1}), \quad \forall k = 0, 1, \dots, K-1, \quad (4)$$

with σ being the nonlinear activation function considered in all layers. We adjust the output layer to enforce the initial conditions x_n by multiplying the PINN output by the step size Δt . This approach ensures numerical consistency and effectively provides an alternative to traditional integration schemes, such as the trapezoidal rule. (5) defines the relation between the differential states at consecutive time steps:

$$\hat{x}_{n+1} = x_n + \Delta t \times (\sigma(W^K z_K + b^K)). \quad (5)$$

B. PINN formulation

The input domain considers the same variables required to solve the underlying block diagram. We classify these inputs into three groups: (i) time step size Δt , (ii) electric systems solution at the current time $\mathbf{x}(t)$, and (iii) the control systems solution at the previous time step $\mathbf{y}(t - \Delta t)$. The output becomes the control systems solution at the current time $\mathbf{y}(t)$. (5) becomes (6), establishing PINNs as an explicit method to capture control systems, as shown in Fig. 5.

$$\hat{\mathbf{y}}_t = \mathbf{y}_{t-\Delta t} + \Delta t \times \text{PINN}(\Delta t, \mathbf{x}_t, \mathbf{y}_{t-\Delta t}). \quad (6)$$

C. Input domain

To enable the systematic reuse of the same PINN across different scenarios and systems, we define an input domain that captures the component dynamics for any given conditions. Thus, the operating ranges of all inputs Δt , $\mathbf{x}(t)$, and $\mathbf{y}(t - \Delta t)$ need to be well represented. For example, the time step size is defined within $\Delta t \in [0, \Delta t_{max}]$. The instantaneous value of voltage waveforms lies within $v_{a,b,c} \in [-1.1V_{nom}, 1.1V_{nom}]$. Control inputs such as the Phase-Locked Loop (PLL) tracked angle lie within $\theta_{pll} \in [0, 2\pi)$. By capturing all possible operating conditions during training, the PINN can solve the trained component in any scenario and system; i.e., the PINN becomes case-independent and can be repeatedly used for faster simulations.

D. Integration

With the presented formulation, PINNs become fully compatible with established simulation frameworks. The formulation maintains the same inputs and outputs, enabling a modular and seamless application. The user can select when and which PINNs to use in a plug-and-play fashion, as PINNs are case-independent and non-exclusive to other traditional numerical schemes. The components replaced by PINNs should have a high computational burden. This enables the user to shift computation to the offline stage, significantly accelerating simulations. As proposed in Fig. 1, PINNs ultimately provide fast and accurate dynamics approximations in exchange for an upfront training cost. Once a PINN is trained for a wide range of operational conditions, the trained PINN can be implemented repeatedly in any scenario, system, or even software.

E. Training procedure

To obtain accurate PINN models, we optimize the training loss function for all weights and biases of the neural network. We utilize a loss function with data-based and physics-based components [9]. The data-based loss, \mathcal{L}_u , minimizes the difference between the target values and the PINN predictions using a mean squared error. These targets are provided by a dataset, \mathcal{D}_u , which contains accurate simulated results for different time step sizes and initial conditions:

$$\mathcal{L}_u = \frac{1}{N_u} \sum_{j=1}^{N_u} \left\| x_{n+1}^j - \hat{x}_{n+1}^j \right\|_2^2. \quad (7)$$

Additionally, we include the underlying equations of the system in training with a physics-based loss \mathcal{L}_p :

$$\mathcal{L}_p = \frac{1}{N_p} \sum_{j=1}^{N_p} \left\| \frac{d}{dt} \hat{x}(t^j) - f(\hat{x}^j, \hat{y}^j) \right\|_2^2. \quad (8)$$

The two loss components are combined with the hyperparameter α , which modulates their contributions. We solve the optimization problem (9) with a gradient-descent algorithm

by adjusting the weights and biases $\{W^k, b^k\}$ of the selected architecture.

$$\min_{\{W^k, b^k\}_{1 \leq k \leq K}} \mathcal{L}_u(\mathcal{D}_u) + \alpha \mathcal{L}_p(\mathcal{D}_p) \quad (9a)$$

$$\text{s.t.} \quad (4), (5). \quad (9b)$$

F. Sensitivity and robustness analysis

In this work, we integrate PINNs into simulation frameworks to reduce the computational burden of specific components and accelerate simulations. To provide accurate approximations that add value, PINNs require rigorous training with a detailed understanding of the models they capture. One of the main aspects to consider is the input domain: PINNs are very accurate at interpolating dynamics within the ranges for which they are trained, but if operating points during a simulation fall beyond the training range, the outputs will quickly become inaccurate. Therefore, on the implementation side, it is essential to verify whether the inputs queried fall within the learned range. A second relevant aspect concerns parameters. PINNs are not as flexible as traditional numerical methods because they are bound to upfront training. Thus, the simulation parameters used in training become fixed for deployment. If any of these parameters need to change in simulations, those parameters should also become PINN inputs. PINNs can capture several inputs and outputs, with the maximum number set by the architecture. Finally, PINNs present limits on how much they can learn based on their architecture and training structure. Training balances how many dynamics are captured and how to parametrize the training details.

V. NUMERICAL TEST RESULTS

This section applies the proposed PINN integration to the EMT simulation framework using a type-4 wind turbine model. We first introduce the case study, followed by the solver and PINN implementation. The numerical results are then compared and analysed, with PSCAD used to validate the results.

A. Study case

We consider an aggregated type-4 wind turbine model connected to an external grid through an LCL filter [25]. We model the grid-side converter as an average controlled voltage source, assuming a constant DC voltage and neglecting the turbine generator and the rotor-side converter. Fig. 6 depicts the control architecture of the considered wind turbine model. A synchronous reference-frame PLL is implemented to synchronize with the external grid. We apply vector control in the dq frame, utilizing a cascaded PI configuration that controls, in the outer loop, the active and reactive power injected into the external grid. We consider an ideal modulation block. The system configuration and parameters are based on the CIGRE benchmark model C4.49 [26]. Table I presents the parameters considered for the wind turbine system.

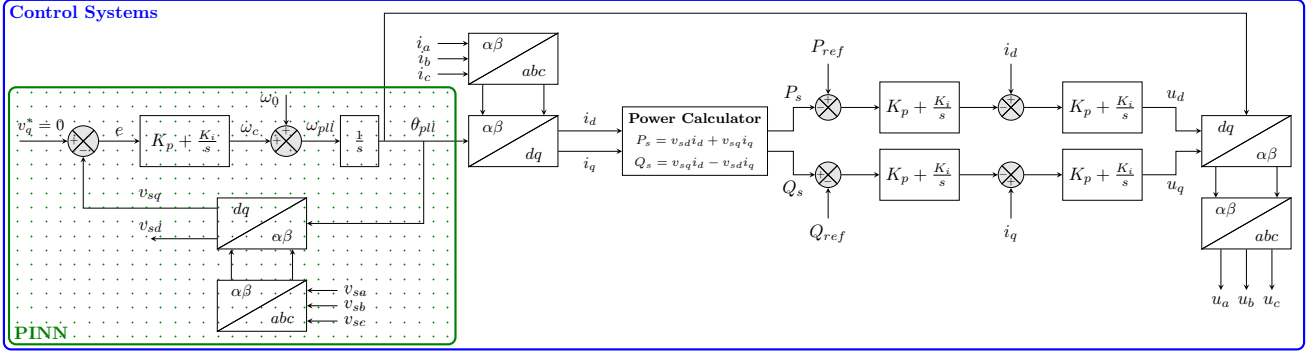


Fig. 6: Block diagram representation of the wind turbine control systems.

TABLE I: System and control parameters

Symbol	Description	Value
S_b	Rated power	100 MW
V_g	Nominal grid voltage	100 kV
f_0	Rated frequency	50 Hz
T_s	Simulation time step size	$\{1-100\} \mu s$
K_{pll}	SRF PLL gains (kp, ki)	25, 300
K_{pc}	Power controller gains (kp, ki)	0.5, 30
K_{cc}	Current controller gains (kp, ki)	0.1, 20
r_c, L_c	Converter-side inductor (pu)	0.005, 0.1
r_f, C_f	Filter capacitor (pu)	0.0757, 0.00184
r_{Lg}, L_g	Grid-side inductor (pu)	0.005, 0.1

B. Study case implementation

We implement the PINN training and integration using the NumPy and Torch libraries [27, 28]. The trained PINN consists of 64 neurons in each of three hidden layers, with the *tanh* activation function. We trained the PINN for 10^6 epochs with the Adam optimizer using a decaying learning rate. Training was performed on an NVIDIA Tesla A100 GPU [29]. The setup parameters were determined empirically, iteratively tuning the architecture and the training algorithm to achieve the most accurate results on a testing dataset. We train the PINN for a broad band of operational conditions, enabling the PINN to be reused across all simulations and scenarios in the subsequent analysis.

C. Comparison methodology

We develop an EMT solver for the described wind turbine model and run it with two configurations: (i) a *traditional* run using a conventional PLL solver (no PINN), and (ii) a *hybrid* run where only the PLL is replaced by a PINN. The rest of the solver remains identical. Both configurations use the same time step size $\Delta t = 100 \mu s$. The *traditional* solver serves as a benchmark for the *hybrid* solver, which evaluates the PLL dynamics using a PINN.

As explained in Sec. III-D, we aim to replace the nonlinear closed loops of the control systems with a PINN to accelerate the simulation solver, thereby avoiding iterative solvers. In the presented wind turbine model, the PLL introduces the only nonlinear closed loop.

D. Simulation results

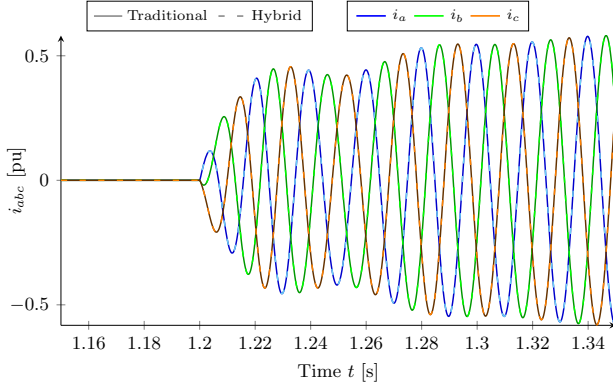
The following analysis shows how integrating PINNs into EMT simulations achieves significant algorithmic acceleration by reducing the computational burden at each time step. We start with a 4-second simulation that introduces an active power step from 0 pu to 0.65 pu at $t = 1.2$ s, a reactive power step from 0 pu to 0.25 pu at $t = 2.2$ s, and a short-circuit for 100 ms in the external grid at $t = 3$ s, decreasing the voltage by 20% of its nominal value. Fig. 7 depicts the converter output currents i_{abc} during the first setpoint step and the voltages v_{abc} during the 100 ms short-circuit using both the *traditional* and *hybrid* algorithms. As we see, the *hybrid* algorithm including the PINN is exactly as accurate as the *traditional* algorithm.

Table II shows the mean absolute error and the largest absolute error of the hybrid algorithm compared to the traditional one for a phase of the currents and voltages. We only show one phase because the operation is balanced. For the presented simulation, we show an acceleration of close to 4.5 times using the hybrid algorithm, without incurring a significant error.

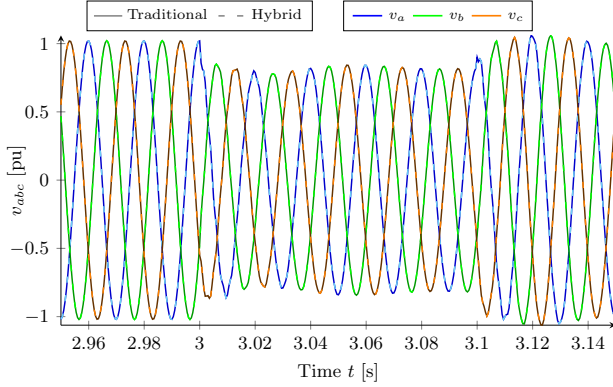
TABLE II: *Hybrid* vs. *traditional*: Speed-up; and mean and maximum errors of system current and voltage

Speed-up	$\ \varepsilon(i_a)\ _1$	$\ \varepsilon(i_a)\ _\infty$	$\ \varepsilon(v_a)\ _1$	$\ \varepsilon(v_a)\ _\infty$
4.24x	$1.77 \cdot 10^{-5}$	$5.1 \cdot 10^{-4}$	$2.30 \cdot 10^{-6}$	$6.04 \cdot 10^{-5}$

Fig. 8 focuses on the control-system solution for the previous simulation, showing the errors and trajectories for the two setpoint steps at $t = 1$ s and $t = 2$ s, followed by a short-circuit at $t = 3$ s. The PLL angle provided by the *hybrid* algorithm introduces a slight shift. A PINN's output, unlike standard equations, yields an approximation of the value it was trained for and not the exact equation solution. However, the introduced shift does not affect the overall performance of the simulation, as the PLL dynamics are calculated with high accuracy. This can be seen in the u_q control trajectory, which is used as an input for the electrical system solution. Since the PLL dynamics captured by the PINN are accurate and stable, the control system output with PINNs can track the dynamics correctly for the whole simulation.



(a) Current injections after active power step.



(b) Voltages at Point of Common Coupling (PCC) during the short-circuit.

Fig. 7: *Traditional* vs *hybrid* algorithms simulation results. Replacing the conventional model of the PLL with a PINN leads to 4.3x speed-up, while maintaining the same accuracy.

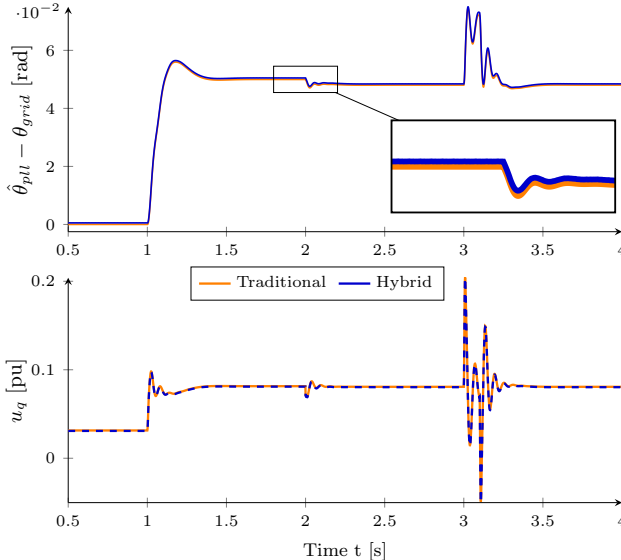


Fig. 8: Simulation results of an active power setpoint change in the wind turbine. Integrating a PINN introduces a speed-up of almost 5 times without significant accuracy loss.

The PINN approximation inaccuracies have a greater impact on the errors in the control system's solution. Tab. III illustrates the magnitudes of these errors, which become slightly more noticeable. However, this slight shift remains small and does not affect the overall performance of the simulation, as they do not propagate over time; it just settles in a steady state that has a slight shift from the PLL. The u_q control trajectory, used as input for the electric system solution, presents a larger peak error but overall captures the dynamics very accurately.

We simulate 20 random operational events using the *traditional* and *hybrid* algorithms and compare their speed and accuracy. These events include changes in active and reactive power setpoints, as well as short circuits on the external grid. Tab. IV provides insights into the acceleration potential of introducing a PINN to explicitly capture the dynamics of the PLL.

VI. CONCLUSIONS

This paper puts forward a vision for leveraging Physics-Informed Neural Networks (PINNs) to accelerate existing power system time-domain simulators. To do so, we identify the most computationally expensive processes in the simulation workflow and train PINN models to replace them with accurate, fast approximations. Following this vision, we present a new PINN formulation that enables a modular, seamless integration into the Electromagnetic Transient (EMT) algorithm, achieving 4x–6x faster results. This means that simulations which would normally take 2 hours to complete, we can now perform them in just 20–30 minutes by replacing a single component (here, a PLL) with a PINN. We illustrate the methodology using a standardized type-4 wind turbine EMT model across multiple scenarios and validate the results with PSCAD. Future work will develop a library of models to enable plug-and-play integration of PINNs into existing open-source and commercial time-domain simulation tools.

Beyond speed, the proposed formulation preserves the simulator interfaces, explicitly replaces nonlinear closed-loop control blocks without time delays or iterative solvers, and maintains high fidelity in both electrical and control trajectories. Still, the approach inherits practical constraints from data- and physics-informed learning: performance depends on the coverage of the training domain and on parameter consistency between training and deployment. Addressing these aspects opens up several interesting research directions. For example, to design processes for (i) automated identification of bottlenecks and selection of models, (ii) replacing several blocks within the same device with separate PINNs, (iii) domain-aware and uncertainty-aware training to guarantee coverage, and (iv) real-time and hardware-in-the-loop validation. As these elements mature, the method proposed in this paper can

TABLE III: *Hybrid* vs. *traditional*: Speed-up; and mean and maximum error for the PLL output

Speed-up	$\ \varepsilon(\theta_{pll})\ _1$	$\ \varepsilon(\theta_{pll})\ _\infty$	$\ \varepsilon(u_q)\ _1$	$\ \varepsilon(u_q)\ _\infty$
4.24x	$4.796 \cdot 10^{-4}$	$9.938 \cdot 10^{-4}$	$4.884 \cdot 10^{-4}$	$1.149 \cdot 10^{-3}$

TABLE IV: *Hybrid* vs. *traditional* for 20 random events: average speed-up; mean and maximum error of system current and voltage averaged over the 20 events

Speed-up	$\ \varepsilon(i_a)\ _1$	$\ \varepsilon(i_a)\ _\infty$	$\ \varepsilon(v_a)\ _1$	$\ \varepsilon(v_a)\ _\infty$
4.87x	$8.884 \cdot 10^{-6}$	$1.754 \cdot 10^{-4}$	$4.92 \cdot 10^{-4}$	$6.88 \cdot 10^{-4}$

generalize across device types and extend from EMT to RMS simulations, providing a unified pathway to scalable, accurate time-domain studies.

APPENDIX

The developed EMT solver used for the numerical results is verified by implementing the same study case in PSCAD. Fig. 9 shows the trajectories obtained with the developed solver and PSCAD for a double setpoint-change trajectory. We apply a 1 s ramp to increase the active power injected into the grid from 0 pu to 1 pu at $t = 2$ s. Three seconds later, at $t = 5$ s, we introduce a setpoint change of injected reactive power from 0 pu to 0.2 pu. We verify that the dynamics and operating points overlap.

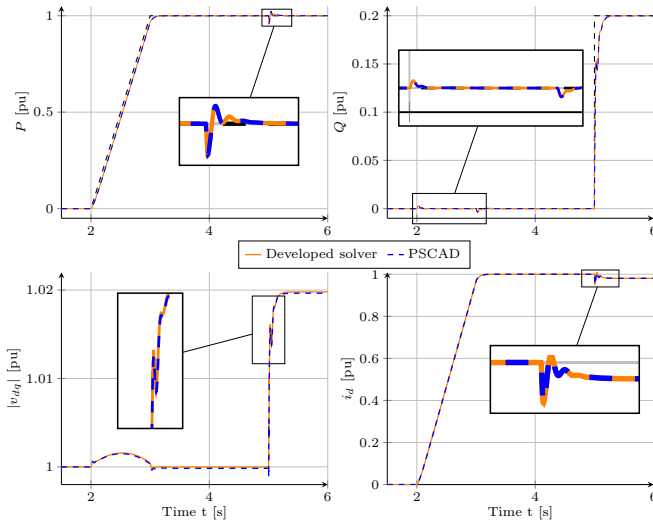


Fig. 9: Power, voltage, and current traces of the study case simulated with the developed solver and PSCAD.

REFERENCES

- [1] N. Hatziaargyriou *et al.*, “Definition and classification of power system stability – revisited & extended,” *IEEE Transactions on Power Systems*, vol. 36, no. 4, pp. 3271–3281, 2021.
- [2] F. Milano, F. Dörfler, G. Hug, D. J. Hill, and G. Verbič, “Foundations and challenges of low-inertia systems (invited paper),” in *2018 Power Systems Computation Conference (PSCC)*, 2018, pp. 1–25.
- [3] B. Stott, “Power system dynamic response calculations,” *Proceedings of the IEEE*, vol. 67, no. 2, pp. 219–241, 1979.
- [4] S. Subedi *et al.*, “Review of methods to accelerate electromagnetic transient simulation of power systems,” *IEEE Access*, vol. 9, pp. 89 714–89 731, 2021.
- [5] B. Bruned, J. Mahseredjian, S. Denettièrre, A. Abusalah, and O. Saad, “Sparse solver application for parallel real-time electromagnetic transient simulations,” *EPSR*, vol. 223, p. 109585, 2023.
- [6] M. D. Omar Faruque *et al.*, “Real-time simulation technologies for power systems design, testing, and analysis,” *IEEE Power and Energy Technology Systems Journal*, vol. 2, no. 2, pp. 63–73, 2015.
- [7] M. Xiong *et al.*, “Paraemt: An open source, parallelizable, and hpc-compatible emt simulator for large-scale ibr-rich power grids,” *IEEE Transactions on Power Delivery*, vol. 39, no. 2, pp. 911–921, 2024.
- [8] J. K. Debnath, A. M. Gole, and W.-K. Fung, “Graphics-processing-unit-based acceleration of electromagnetic transients simulation,” *IEEE Transactions on Power Delivery*, vol. 31, no. 5, pp. 2036–2044, 2016.
- [9] M. Raissi, P. Perdikaris, and G. Karniadakis, “Physics-informed neural networks: A deep learning framework for solving forward and inverse problems involving nonlinear partial differential equations,” *Journal of Computational Physics*, vol. 378, pp. 686–707, 2019.
- [10] C. Legaard *et al.*, “Constructing neural network based models for simulating dynamical systems,” *ACM Comput. Surv.*, vol. 55, no. 11, 2023. [Online]. Available: <https://doi.org/10.1145/3567591>
- [11] J. Stiasny, B. Zhang, and S. Chatzivasileiadis, “Pinnsim: A simulator for power system dynamics based on physics-informed neural networks,” *Electric Power Systems Research (EPSR)*, vol. 235, p. 110796, 2024.
- [12] I. Ventura, J. Stiasny, and S. Chatzivasileiadis, “Physics-informed neural networks: A plug and play integration into power system dynamic simulations,” *EPSR*, vol. 248, p. 111885, 2025.
- [13] C. Moya and G. Lin, “Dae-pinn: a physics-informed neural network model for simulating differential algebraic equations with application to power networks,” *Neural Comput & Applic* 35, p. 3789–3804, 2023.
- [14] I. Ventura, R. Nellikkath, and S. Chatzivasileiadis, “Physics-informed neural networks in power system dynamics: Improving simulation accuracy,” in *2025 IEEE Kiel PowerTech*, 2025, pp. 1–6.
- [15] I. Ventura, “PINNs for EMT,” <https://github.com/ignvenad/PINNs-for-EMT>, 2025.
- [16] J. D. Lara *et al.*, “Revisiting power systems time-domain simulation methods and models,” *IEEE Transactions on Power Systems*, vol. 39, no. 2, pp. 2421–2437, 2024.
- [17] K. E. Brenan, S. L. Campbell, and L. R. Petzold, *Numerical Solution of Initial-Value Problems in Differential-Algebraic Equations*. Society for Industrial and Applied Mathematics, 1995.
- [18] J. Martinez-Velasco, *Transient Analysis of Power Systems: A Practical Approach*. John Wiley & Sons, Ltd, 2020.
- [19] H. W. Dommel, “Digital computer solution of electromagnetic transients in single-and multiphase networks,” *IEEE Transactions on Power Apparatus and Systems*, vol. PAS-88, no. 4, pp. 388–399, 1969.
- [20] H. Dommel, *Electromagnetic Transients Program. Reference Manual (EMTP Theory Book)*. Portland (OR, USA): Bonneville Power Administration, 1986.
- [21] L. Dubé and H. W. Dommel, “Simulation of control systems in an electromagnetic transients program with tacs,” *IEEE Power Industry Computer Applications Conf.*, p. 266–271, 1977.
- [22] A. Araujo, H. Dommel, and J. Marti, “Simultaneous solution of power and control systems equations,” *IEEE Transactions on Power Systems*, vol. 8, no. 4, pp. 1483–1489, 1993.
- [23] J. Mahseredjian, L. Dube, M. Zou, S. Denettièrre, and G. Joos, “Simultaneous solution of control system equations in emtp,” *IEEE Transactions on Power Systems*, vol. 21, no. 1, pp. 117–124, 2006.
- [24] I. Goodfellow, Y. Bengio, and A. Courville, *Deep Learning*. MIT Press, 2016. <http://www.deeplearningbook.org>.
- [25] M. K. Bakhshizadeh, S. Ghosh, L. Kocewiak, and G. Yang, “Improved reduced-order model for pll instability investigations,” *IEEE Access*, vol. 11, pp. 72 400–72 408, 2023.
- [26] L. Kocewiak *et al.*, “Overview, status and outline of stability analysis in converter-based power systems,” in *Proc. 19th Int. Workshop Large-Scale Integr. Wind Power Into Power Syst.*, 2020.
- [27] C. R. Harris *et al.*, “Array programming with NumPy,” *Nature*, vol. 585, no. 7825, pp. 357–362, Sep. 2020.
- [28] A. Paszke *et al.*, “Pytorch: An imperative style, high-performance deep learning library,” in *Advances in Neural Information Processing Systems*, vol. 32. Curran Associates, Inc., 2019.
- [29] DTU Computing Center, “DTU Computing Center resources,” 2024. [Online]. Available: <https://doi.org/10.48714/DTU.HPC.0001>